Phys. Status Solidi A **208**, No. 10, 2430–2436 (2011) / **DOI** 10.1002/pssa.201026534

physica status solidi a
www.pss-a.com
applications and materials science

Experimental study of iron redistribution between bulk defects and boron doped layer in silicon wafers

Heli Talvitie*, Marko Yli-Koski, Antti Haarahiltunen, Ville Vähänissi, Muhammad Imran Asghar, and Hele Savin

Department of Micro and Nanosciences, Aalto University, P.O. Box 13500, FI-00076 Aalto, Espoo, Finland

Received 3 September 2010, revised 10 May 2011, accepted 6 June 2011
Published online 7 July 2011

Keywords boron doping, defects, iron gettering, silicon

* Corresponding author: e-mail heli.talvitie@aalto.fi, Phone: +358-9-47024987, Fax: +358-9-47025008

We have studied iron distribution between a boron-implanted (p+) layer and bulk defects in single crystalline silicon wafers after various gettering anneals. Our results show that iron accumulation into the p+ layer was pronounced after each anneal. However, we were able to decrease the strong accumulation by combining a specific low-high anneal with high bulk defect density. We determined the dominant mechanism behind the accumulation of iron into the p+ layer, which turned out to be precipitation instead of segregation. The results can be helpful when choosing the internal gettering steps for both microelectronic (IC) and multicrystalline silicon photovoltaic (PV) processes.

1 Introduction Internal gettering is a technique, which has been used in microelectronics (IC) to remove detrimental 3d transition metals from the region near the surface of Czochralski-grown silicon wafers and capture them to oxide precipitates and related defects in the wafer bulk [1–8]. Naturally, the removal of minority carrier lifetime degrading impurities, such as iron, from the device layer improves the IC device performance.

Internal gettering has recently drawn attention also in photovoltaics (PV) [9, 10], although the basic idea is quite different from IC: in PV cells the device area extends through the wafer and therefore it is important to have a high minority carrier lifetime also in the wafer bulk. Conventionally, this is achieved by removing the harmful metals from the bulk. A more recent approach is to keep the metals in the bulk but change them to a less recombination active form [11]. For instance, iron is less detrimental in precipitated than in dissolved form. This fact can be utilized especially in multicrystalline silicon since the dissolved iron concentration can be reduced by precipitating iron to the bulk defects. Indeed, recent studies have shown that such internal gettering can improve the performance of multicrystalline silicon solar cells [9].

Both in IC and PV devices iron tends to segregate to highly doped regions [12]. This is a harmful effect especially in IC: iron increases, e.g. the pn-junction leakage current and thus deteriorates the device performance. In PV, the effect is usually beneficial as the metal contamination decreases in the bulk resulting in higher bulk lifetime. On the other hand, if iron is removed from the bulk and gettered in dissolved form to the heavily doped emitter, it can increase the emitter saturation current, which reduces the cell performance [13].

In this work we continue our previous studies [14], where the purpose was to reduce the harmful iron accumulation into the p+ layer by maximizing the iron precipitation at bulk defects. There we discovered that in certain conditions it is possible to achieve a slight decrease in the iron contamination in a heavily doped p+ layer, but the optimization of such a gettering process was considered demanding. Here we study further the iron behaviour in similar samples. We make several gettering anneals and measure both the dissolved and total iron concentrations in the wafers with various characterization methods. The results are compared with simulations. Finally, we can discuss more comprehensively the physical mechanisms behind the iron gettering by boron implantation.

2 Background for the gettering anneals A necessary prerequisite for internal gettering is the nucleation of iron at gettering sites in the wafer bulk [7]. We can

maximize the iron nucleation using so-called two-step (low-high) anneal [15]. The first step nucleates iron at bulk defects, which requires a rather low temperature. The second step increases iron capture in the bulk by growing iron precipitates at a higher temperature. An alternative to the low-temperature anneal is a simple temperature ramp, e.g. to room temperature (RT step). Note that the nucleation depends strongly on both the iron contamination level and processing temperature, i.e. the supersaturation level [16].

The low-high anneal was shown to be effective in homogeneously doped wafers, i.e. when no p+ layer is present. However, the p+ layer may change the iron behaviour due to segregation. The segregation coefficient is high during the low-temperature step but, on the other hand, the diffusion is slow. During the following high-temperature step, the segregation is reduced and we can assume that the precipitation in the bulk dominates in most cases. We can thus conclude that most of the iron should remain in the bulk after the appropriate low-high anneal also in the presence of the p+ layer. This hypothesis was confirmed by simulations (shown later), which revealed that the iron concentration in the p+ layer was dramatically reduced in samples with bulk defects. In the following, we study if the experiments can support the above hypothesis or possibly reveal features in iron behaviour that are not apparent based on previous studies.

3 Experimental and modelling details

3.1 Sample preparation Samples used in the experiments were Czochralski-grown (100)-oriented boron doped silicon wafers with a diameter of 100 mm. Different heat treatments were applied (Table 1) in order to get wafers with different denuded zone (DZ) widths near the wafer surface and different bulk microdefect (BMD), i.e. internal gettering site, densities in the wafer bulk. Oxygen loss during the heat treatments was measured by Fourier transform infrared spectroscopy (FTIR). Using iterative diffusion limited growth method [17] to fit the measured oxygen loss, the BMD density and radius given in Table 1 were obtained. This method has been shown to correlate well with preferential etching results [18]. In this calculation the solubility and diffusivity values for oxygen were taken from Ref. [19] and SiO phase was assumed [20]. The oxygen out-diffusion during the first high-temperature anneal at 1150 °C was also taken into account (0.5 or 1 ppma for 4 or 16 h anneal, respectively). The values for the DZ width are based on the duration of the first high-temperature anneal [21].

Table 1 Oxygen precipitation heat treatments for various samples and resulting bulk defect density (BMD density), bulk defect radius (BMD radius) and denuded zone width (DZ).

samples	heat treatment	BMD density (cm^{-3})	BMD radius (nm)	DZ (μm)
A1	4 h at 1150 °C +6 h at 650 °C +16 h at 1100 °C	4.2×10^9	97	40–50
A2	4 h at 1150 °C +2 h at 650 °C +16 h at 1100 °C	3.6×10^9	100	40–50
B	16 h at 1150 °C +2 h at 550 °C +16 h at 1100 °C	3.4×10^9	100	60–80
C1	4 h at 1150 °C	1.2×10^8	83	40–50
C2	16 h at 1150 °C	1.2×10^8	162	70–100
D	no heat treatment	–	–	–

Thickness of the wafers was 625 μm, resistivity 30 Ωcm and interstitial oxygen concentration 16 ppma (ASTM F 121-83 standard). For comparison, also wafers without any oxygen precipitation heat treatment were prepared. Their thickness was 525 μm, resistivity 21 Ωcm and interstitial oxygen concentration less than 8 ppma (ASTM F 121-83 standard).

All wafers were contaminated with iron by immersing them in an SC1 solution, which contained an addition of $FeCl_3 \cdot 6H_2O$. The iron concentration of the final solution was 30 ppb. Subsequently, iron was diffused into the wafers at 850 °C for 55 min, after which the surface iron contamination was removed in an $HF:H_2O_2:H_2O$ solution. After iron in-diffusion, a 26 nm thick pad oxide for boron implantation was grown on the wafers by a 20 min dry oxidation at 1000 °C. The iron concentration was then determined to be $1.7 \times 10^{13}\,cm^{-3}$ by microwave detected photoconductance decay (μPCD) measurement. When this iron concentration is initially homogeneously distributed through the wafer, it corresponds to concentration of $4 \times 10^9\,cm^{-2}$ within the 2.4 μm thick layer at the wafer surface. This is the layer thickness, which is later used for monitoring total iron concentration. A boron dose of $1 \times 10^{15}\,cm^{-2}$ was implanted on the front side of the wafers with an energy of 40 keV through the pad oxide, which was removed after implantation in a diluted HF solution. Wafers were cleaned in the sequence of standard wafer cleaning solutions SC1 and SC2 including a dip in diluted HF as the last step. Boron implantation activation treatment included dry oxidation at 1000 °C for 15 min, annealing at 1000 °C for 25 min, cooling at a rate of 4 °C/min down to 800 °C and unloading to RT, which resulted in a 23 nm thick oxide.

Finally, various low-temperature anneals were applied in N_2 ambient to wafer sets consisting of wafers with different oxide precipitate profiles. We selected the specific two-step anneal, RT + 700 °C, from previously published experiments as the basis for all our experiments. In Ref. [15] pulling the samples from oxidation at 900 °C quickly to room temperature (RT step) followed by an anneal at 700 °C resulted in effective internal gettering with the relevant contamination level. Table 2 presents the four different anneals examined in this study and anneal notations for each anneal. Note that the 700–450 samples are the same samples presented in Ref. [14], only a bit different notations were then used. To test the possible iron diffusion to the wafer surfaces, also some wafers without bulk defects and implanted boron layer were prepared and annealed with the 270–700 anneal.

Table 2 Details of the low-temperature anneals.

anneal notation	low-temperature anneal
450	RT + 1 h at 450 °C
700–450	RT + 1 h at 700 °C + RT + 1 h at 450 °C
450–700	RT + 1 h at 450 °C + 1 h at 700 °C
270–700	RT + 1 h at 270 °C + RT + 1 h at 700 °C

3.2 Measurements The total iron content in the silicon dioxide layer on the wafer front surface and at the interface between silicon dioxide and silicon was determined from the wafer centre by vapour phase decomposition (VPD) and total reflection X-ray fluorescence (TXRF) technique [22, 23]. Subsequently, the iron content in the implanted boron layer (p+) of the same wafers was determined by etching a thickness of 2.4 μm from the front surface using drop sandwich etching (DSE) technique [22, 24]. The etching solution residue was analyzed by TXRF technique. The detection limit of the measurement was about 3×10^{10} cm^{-2}, which was determined by measuring several clean reference wafers. The error estimate is 20% for the determined iron content value in the p+ layer.

Iron concentration in the bulk of selected wafers was measured with deep level transient spectroscopy (DLTS). A thickness of 50 μm from the wafer surfaces was etched in a $HF:HNO_3:CH_3COOH$ solution. Wafers were cut into pieces and contacts were prepared on these samples to measure the dissolved iron concentrations both from the front and from the back side of the wafers.

3.3 Modelling In the simulations, we take into account both iron precipitation to crystal defects and segregation to the p+ layer. Iron precipitation is simulated using a model presented in Refs. [16, 25], which takes into account the heterogeneous nucleation of iron by special growth and dissolution rates. In the simulations of diffusion and segregation of iron to the p+ layer we use an algorithm described in Ref. [26], which includes both the dependence of iron solubility on boron doping [27] and the dependence of iron diffusivity on trapping of ionized interstitial iron by boron [28]. The boron concentration profile was simulated with Icecrem 4.3 software. The maximum boron concentration was 2×10^{19} cm^{-3} and the thickness of the p+ layer is around 900 nm. The simulated boron profile is shown in Fig. 2c. During the low-temperature anneals, boron diffusion was neglected due to the low diffusivity of boron at these temperatures.

4 Results

4.1 Iron concentration in the p+ layer The first experiment is related to the sensitivity of the droplet sandwich etching technique (DSE), which we use to measure the total iron concentration in the p+ layer. DSE has a rather high detection limit, 3×10^{10} cm^{-2}, and therefore we first want to find an anneal which would result in high enough segregation for reliable detection of iron in the p+ layer. The results shown in Fig. 1a reveal that after 1 h anneal at 450 °C we have a high enough iron concentration in the p+ layer, but not all iron is collected from the bulk due to the limited diffusion length of iron (90 μm). For comparison, with the used wafer thickness and initial iron contamination level, the iron concentration would be about 8.9×10^{11} cm^{-2} when all the iron has been accumulated into the p+ layer. The results also show that the bulk defects do not affect the iron segregation much at 450 °C.

The second experiment was made to test our hypothesis that if we capture the mobile iron in the bulk by the low-high anneal (RT + 700 °C), iron cannot segregate any more into the p+ layer at 450 °C. The experiments reveal (Fig. 1b) that in such anneal the presence of bulk defects (samples A–C)

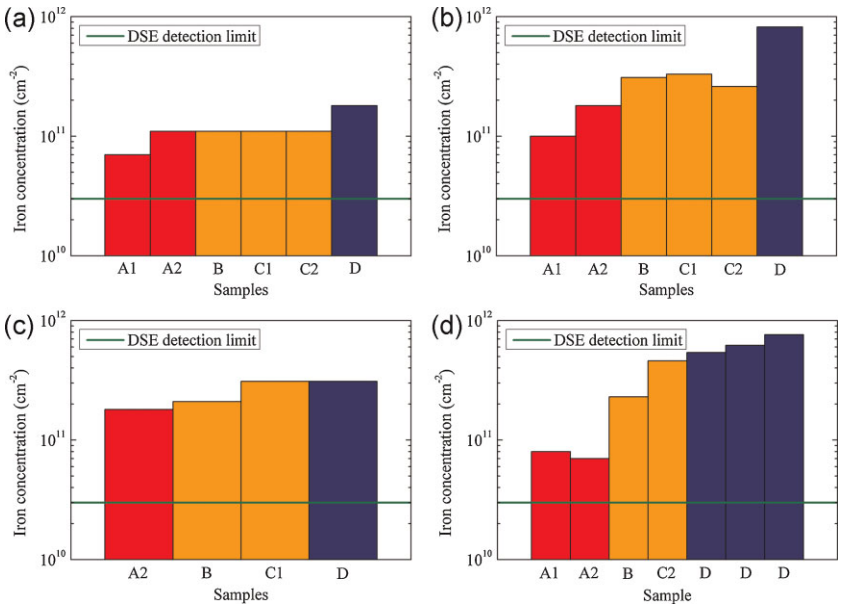

Figure 1 (online colour at: www.pss-a.com) Measured iron concentrations in the 2.4 μm thick layer on the wafer surface including the p+ layer after low-temperature anneal (a) 450, (b) 700–450, (c) 450–700 and (d) 270–700. For comparison, the initial iron concentration in the 2.4 μm thick surface layer was about 4×10^9 cm^{-2}.

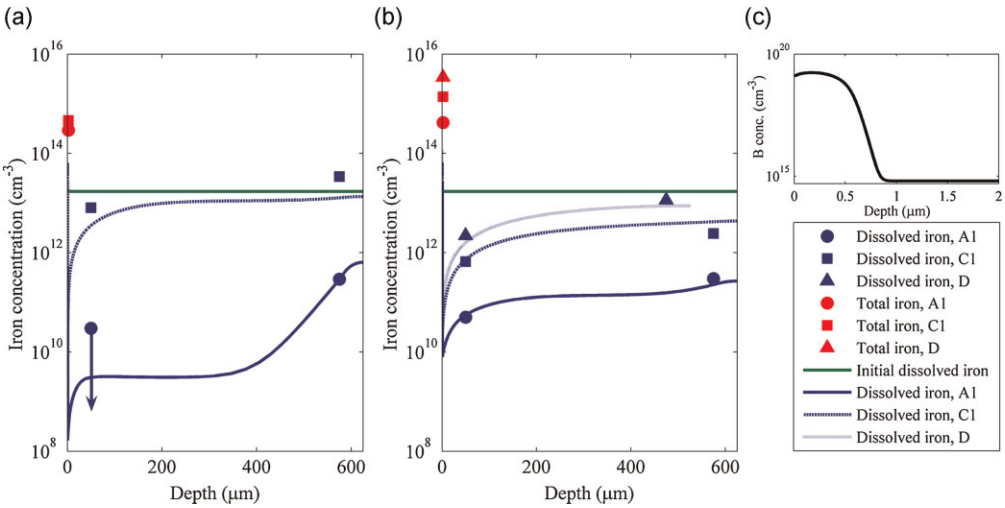

Figure 2 (online colour at: www.pss-a.com) Experimental (blue symbols) and simulated (blue lines) dissolved iron concentrations through the wafer thickness after low-temperature anneal (a) 450 and (b) 700–450. Samples with high and low bulk defect densities (A1 and C1, respectively) and without bulk defects (D) are shown. The data point of dissolved iron concentration at 50 μm depth after the 450 anneal is below the detection limit. Total iron contents in the p+ layer from the DSE measurements, which are converted to average bulk concentrations in the 2.4 μm thick layer from the wafer surface (red symbols), are also shown. In simulations, the bulk defect density was 4×10^9 cm^{-3} for A1 samples and 1.2×10^8 cm^{-3} for C1 samples. Denuded zone width (DZ) was 40 μm for A1 and C1 and 525 μm for D samples. (c) The simulated boron concentration profile.

indeed decreases the accumulation of iron into the p+ layer compared to sample D. It is interesting to notice that in the D sample the iron concentration is 8.2×10^{11} cm^{-2}, which means that at 700 °C a quite significant amount of iron has been gettered to the p+ layer.

Even though the RT + 700 °C step increased the difference between samples A–C and D, a quite considerable amount of iron was still detected in the p+ layer. Therefore, we tried to enhance the nucleation in the bulk by decreasing the temperature of the first step to 450 °C. The results of this 450–700 anneal are presented in Fig. 1c. This anneal resulted in iron concentrations in the p+ layer which were even higher, about double, compared to the iron concentrations after the 450 anneal. These results imply that iron did not precipitate at 450 °C in the bulk but instead more iron was able to accumulate into the p+ layer during the following anneal at 700 °C. The physical mechanism and the explanation for these results are discussed later on in this paper.

In the last experiment, we reduced the nucleation temperature, i.e. the first step of the gettering anneal, even further to 270 °C, to induce faster iron nucleation in the bulk. This should be a low enough temperature to reduce the iron flux to the p+ layer, despite the fact that the segregation coefficient is increased. As seen from Fig. 1d, this experiment shows that it is possible to drastically reduce the iron concentration in the p+ layer by internal gettering, though a high bulk defect density is required.

In general, in the A samples, with high bulk defect density and narrow DZ, the lowest iron concentrations in the p+ layer were indeed achieved by combining iron precipitate nucleation anneal at 270 °C and growth anneal at 700 °C. In the B and C samples the lowest iron concentrations in the p+ layer were achieved after a mere 450 anneal. During all other anneals, the step at 700 °C seems to slowly collect iron into the p+ layer.

4.2 Iron concentration in the bulk The bulk iron concentrations were measured by DLTS in order to see if they are in agreement with the DSE results. It is important to note that the DSE measurement gives the total iron concentration whereas DLTS measures the dissolved iron concentration. Figure 2 presents the DLTS results at 50 μm depth from the wafer front and back surfaces along with the simulated dissolved iron concentrations through the wafer.

The deep level transient spectroscopy results support the DSE measurements of the p+ layer, which are also shown for comparison in Fig. 2. As presented in the previous chapter, iron precipitation to the bulk defects decreases the total iron concentration in the p+ layer. Similarly, the DLTS results show that because of iron precipitation to the bulk defects, the dissolved iron concentrations in the bulk are lower in the samples that have lower total iron concentration in the p+ layer. A gradient is seen in the dissolved bulk iron concentration because the iron segregation into the p+ layer decreases the dissolved bulk iron concentration towards the front surface. The increase in the dissolved iron concentration near the back surface seen in the A1 samples is only due to the DZ which is also present at the wafer back side.

The deep level transient spectroscopy results also reveal some information which is not detectable from the DSE results. After the 450 anneal the total iron concentrations in the p+ layers of A1 and C1 samples are about the same, but there is a pronounced difference between the dissolved bulk

iron concentrations: the dissolved iron concentration has decreased several orders of magnitude in the bulk of the A1 sample while in the C1 sample the dissolved iron concentration is nearly the same as the initial value. This implies that iron precipitation in the bulk is much faster in the A1 sample than in the C1 sample. Note that the higher mobile iron concentration in C1 samples does not accumulate more iron into the p+ layer due to the small diffusion length of iron in 1 h anneal at 450 °C. Iron is mainly collected to the p+ layer from the depth less than 100 μm, which contains the DZ and therefore less bulk defects. Consequently, iron is collected to the p+ layer in sample A1 nearly as efficiently as in sample C1.

There is also a similar difference between dissolved bulk iron concentrations in A1 and C1 samples after the 700–450 anneal. The anneal at 700 °C decreases the dissolved bulk iron concentration to about 1×10^{12} cm^{-3}, but the anneal at 450 °C decreases it further only in the A1 sample. In the D samples without any bulk defects, the dissolved concentration remains close to the initial value. On the whole, the DLTS results show that iron has indeed precipitated in the bulk of A–C samples; the DSE measurements just were not able to reveal that.

4.3 Iron concentration in the Si–SiO_2 interface

To investigate the possible iron diffusion to the wafer surface, we measured the iron concentration in the front SiO_2 layer including the SiO_2–Si interface above the p+ layer. A sample without the p+ layer (no p+) and bulk defects (no BMD) was added to study the roles of the p+ layer and bulk defects in the iron diffusion to the surface. Figure 3 presents the VPD measurement results after the 270–700 anneal. When there are no p+ layer or bulk defects present, a significant amount of iron has accumulated at a very thin wafer surface layer on the front side, and most probably also on the back side, of the wafer. Therefore, in the absence of the p+ layer and bulk defects, iron accumulation to the surface cannot be neglected [29].

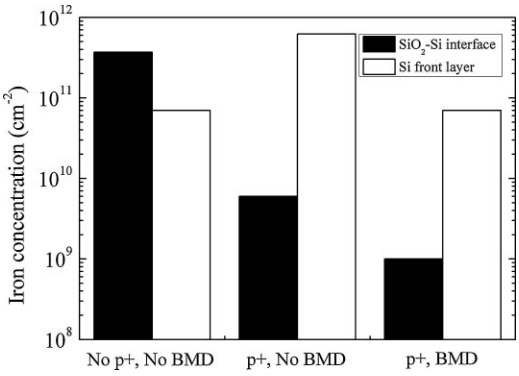

Figure 3 Iron concentrations in (i) SiO_2 layer and SiO_2–Si interface (denoted as SiO_2–Si interface) and (ii) in the 2.4 μm thick silicon front layer measured by DSE. Samples (i) without the p+ layer and bulk defects (no p+, no BMD), (ii) with the p+ layer and without the bulk defects (p+, no BMD) and (iii) with the p+ layer and bulk defects (p+, BMD), after the 270–700 anneal are shown.

The presence of a p+ layer changes the iron distribution near the wafer surface so that iron is primarily present in the p+ layer (Fig. 3). It should be noted that the DSE result gives the total iron concentration in the p+ layer but no information about the iron distribution over the measured thickness. One possibility is that iron is located near the wafer surface, but over a wider range compared to the wafer without the p+ layer. Overall, the results indicate that in our experiments iron does not accumulate significantly into the SiO_2 layer or the SiO_2–Si interface. Similar results were obtained in all the other low-temperature anneal samples (results not shown here).

5 Discussion Here we discuss the interpretation of the experiments and compare the results to previously published data. It is widely accepted that a heavily doped boron layer acts as an efficient sink for iron due to segregation. Indeed, in our hypothesis the segregation was considered to be the only mechanism, which collects iron to the p+ layer. However, the relatively high iron concentrations measured in the p+ layer after each low-temperature anneal suggest that the segregation effect is not the only mechanism that collects iron to the p+ layer.

It seems quite likely that iron has also precipitated in the p+ layer. This is still quite unexpected as ion implantation induced defects, which could serve as precipitation sites for iron, were assumed to anneal out after implantation. The low implantation dose and energy used in the experiments should not cause significant damage, i.e. nucleation sites for iron. Boron concentration was also so low that we considered it unlikely that boron would form B–Si precipitates which could be efficient gettering sites for iron [30, 31].

Nevertheless, the gettering mechanism can be rather easily checked by simulations. The results are shown in Fig. 4. It clearly shows that the experiments agree with simulations when the precipitation in the p+ layer is included. The high iron concentrations measured in A–C

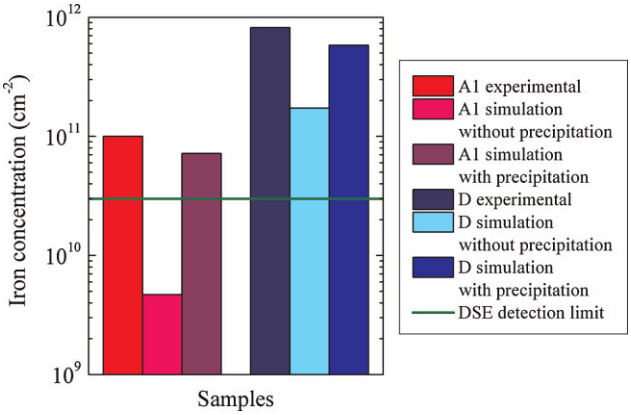

Figure 4 (online colour at: www.pss-a.com) Experimental and simulated iron concentrations in the p+ layer after low-temperature anneal 700–450. Iron precipitation in the p+ layer was either taken into account or neglected in the simulations. Precipitation parameters are given in the text.

samples can thus be explained by the strong precipitation in the p+ layer, which in these samples competes with the precipitation in the bulk. The simulation of the precipitation in the p+ layer was realized using the approach given in Refs. [14, 32]. Iron precipitation in the boron implanted layer was simulated using 100 nm thick defect layer at the wafer surface with precipitation site density of $5 \times 10^{12}\,\mathrm{cm}^{-3}$ and radius of 15 nm. In A1 samples the bulk defect density was $4 \times 10^{9}\,\mathrm{cm}^{-3}$ and in C1 samples $1.2 \times 10^{8}\,\mathrm{cm}^{-3}$. In both cases, the radius of bulk defects was 30 nm and DZ was 40 μm. In D samples the zero bulk defect density was assumed. A ramp rate of 500 °C/min was assumed during cooling from high temperature to RT after the boron implantation. Ramps in other process steps were neglected.

The iron precipitation in the p+ layer can also explain the DSE results of the 450–700 anneal. Due to the segregation at 450 °C the interstitial iron concentration is much (a factor of k_{seg}) higher in the p+ layer than in the bulk. However, the supersaturation in the bulk decreases only slightly because the p+ layer is very thin compared to the bulk. This leads to faster nucleation rate of iron in the p+ layer than in the bulk [12, 33]. During the following rather slow ramp up and anneal at 700 °C, iron precipitates grow in the p+ layer instead of precipitating in the bulk, which results in strong accumulation of iron into the p+ layer (Fig. 1c). It should be noted that the very low dissolved iron concentration measured in the bulk of the A1 sample after the 450 anneal (Fig. 2a) suggests that iron precipitates also significantly in the bulk. Unfortunately, in the 450–700 anneal we did not have an A1 sample, which could confirm this speculation.

Finally, reducing the temperature of the nucleation step to 270 °C decreased the iron accumulation into the p+ layer, although the precipitation in the p+ layer could not be totally avoided. At 270 °C, the segregation coefficient is increased but the diffusion length of iron is limited, which results in a higher driving force for iron nucleation in the bulk than in the p+ layer. In general, a high bulk defect density is required in addition to the low nucleation temperature to reduce the accumulation of iron into the p+ layer.

It should be kept in mind that the initial contamination level plays a role in the selection of the nucleation and growth temperatures. If we aim to minimize the iron concentration in the p+ layer, the nucleation temperature should be chosen low enough and bulk defect density high enough to induce faster nucleation of iron precipitates in the bulk than in the p+ layer. The growth temperature should be high enough in order to decrease the segregation to the p+ layer but low enough in order to prevent iron precipitate dissolution in the bulk.

Similar results of strong iron accumulation into the boron doped region as those obtained in our work can be found in the literature. Benton et al. [34–36] studied iron gettering by high energy boron implantation in float zone silicon samples with the iron contamination level of $2 \times 10^{14}\,\mathrm{cm}^{-3}$. Their samples received an anneal at 1000 °C after the boron implantation and some samples received also an additional anneal between 600 and 1000 °C. They observed that with extended annealing at 600 or 800 °C almost all iron was collected to the boron doped layer. They could only explain the results with the iron precipitation mechanism, which is in agreement with our results.

Benton et al. [34] also studied the boron implantation gettering after fast cooling from 1000 °C. In these samples, iron was gettered to the p+ layer only from the nearby area and the bulk iron concentration remained at the initial level. These results were explained by the segregation mechanism. During cooling from 1000 °C, the iron precipitation rate in the p+ layer is so slow that it is masked by the segregation, which is an instantaneous mechanism.

Generally, the dominating gettering mechanism depends on the anneal conditions. Clearly, a short anneal at low temperatures, such as our 1 h anneal at 450 °C or a fast cooling, such as in the experiments by Benton et al., leads to an unsteady state, which means that a sufficient time has not yet elapsed for iron precipitates to nucleate. Therefore, diffusion and segregation are the dominant mechanisms behind the iron accumulation into the p+ layer. During the extended anneal, on the contrary, the steady state is nearly reached and many iron precipitates are formed. Consequently, diffusion and precipitate growth rate, rather than the nucleation rate, limit the iron accumulation into the p+ layer. As the latter conditions apply to most of our anneals, mere segregation is not enough to explain the iron accumulation into the p+ layer.

6 Conclusions We have studied experimentally competitive gettering of iron in single crystalline silicon wafers where both bulk defects and an implanted boron layer near the wafer surface were present. We performed various gettering anneals and measured both the dissolved and total iron concentrations in the wafers to gain a deeper understanding of the physical mechanisms behind the strong iron accumulation into a boron-implanted layer.

Specific low-temperature anneals were found to give rise to iron gettering to the bulk defects and thus to reduce the iron concentration in the p+ layer. Iron concentration in the boron doped layer was measured to be lowest after an anneal for 1 h at 270 °C + 1 h at 700 °C. The low-temperature step at 270 °C was applied to create a higher density of iron precipitate nuclei in the wafer bulk compared to the p+ layer. The following high-temperature step at 700 °C was applied to grow the iron precipitates. The effect was most pronounced in wafers where the bulk defect density was high and the DZ was narrow. Presumably iron would behave in the same way also in multicrystalline silicon as these samples resemble multicrystalline silicon with a large amount of precipitation sites in the bulk. From the PV point of view, p+ layer seems to be efficient gettering site in almost all conditions. Depending on the application (IC *vs.* PV) the desired location of iron may be either the bulk or the p+ layer. This can be engineered by choosing an appropriate anneal as presented here.

All in all, we have found that iron precipitation to the bulk defects cannot entirely prevent the accumulation of iron into the p+ layer. We have discussed the possible gettering

mechanisms and came to the conclusion that in our experiments the dominant mechanism behind the strong accumulation of iron into the p+ layer is iron precipitation.

Acknowledgements The authors acknowledge the financial support from the Finnish National Technology Agency, Academy of Finland, Micro Analog Systems Oy, Okmetic Oyj, Endeas Oy, Semilab Inc. and VTI Technologies Oy.

References

[1] T. Y. Tan, E. E. Gardner, and W. K. Tice, Appl. Phys. Lett. **30**, 175 (1977).
[2] D. Gilles, E. R. Weber, and S. K. Hahn, Phys. Rev. Lett. **64**, 196 (1990).
[3] M. Aoki, A. Hara, and A. Ohsawa, Jpn. J. Appl. Phys. **30**, 3580 (1991).
[4] M. Aoki, A. Hara, and A. Ohsawa, J. Appl. Phys. **72**, 895 (1992).
[5] S. A. McHugo, E. R. Weber, M. Mizuno, and F. G. Kirscht, Appl. Phys. Lett. **66**, 2840 (1995).
[6] S. Ogushi, S. Sadamitsu, K. Marsden, Y. Koike, and M. Sano, Jpn. J. Appl. Phys. **36**, 6601 (1997).
[7] H. Hieslmair, A. A. Istratov, S. A. McHugo, C. Flink, T. Heiser, and E. R. Weber, Appl. Phys. Lett. **72**, 1460 (1998).
[8] H. Takahashi, H. Yamada-Kaneta, and M. Suezawa, Jpn. J. Appl. Phys. **37**, 1689 (1998).
[9] M. D. Pickett and T. Buonassisi, Appl. Phys. Lett. **92**, 122103 (2008).
[10] M. Rinio, A. Yodyunyong, S. Keipert-Colberg, Y. P. Botchak Mouafi, D. Borchert, and A. Montesdeoca-Santana, Prog. Photovolt. Res. Appl. **19**, 165 (2011).
[11] T. Buonassisi, A. A. Istratov, M. A. Marcus, B. Lai, Z. Cai, S. M. Heald, and E. R. Weber, Nature Mater. **4**, 676 (2005).
[12] D. Gilles, W. Schröter, and W. Bergholz, Phys. Rev. B **41**, 5770 (1990).
[13] D. Macdonald, H. Mäckel, and A. Cuevas, Appl. Phys. Lett. **88**, 092105 (2006).
[14] M. I. Asghar, M. Yli-Koski, H. Savin, A. Haarahiltunen, H. Talvitie, and J. Sinkkonen, Mater. Sci. Eng. B **159–160**, 224 (2009).
[15] H. Väinölä, A. Haarahiltunen, E. Saarnilehto, M. Yli-Koski, J. Sinkkonen, and O. Anttila, in: High Purity Silicon VIII, edited by C. L. Claeys, M. Watanabe, R. Falster, and P. Stallhofer (The Electrochemical Society, Pennington, New Jersey, USA, 2004), pp. 160–164.
[16] A. Haarahiltunen, H. Väinölä, O. Anttila, M. Yli-Koski, and J. Sinkkonen, J. Appl. Phys. **101**, 043507 (2007).
[17] H. Hieslmair, A. A. Istratov, T. Heiser, and E. R. Weber, J. Appl. Phys. **84**, 713 (1998).
[18] J. P. Joly and V. Robert, Semicond. Sci. Technol. **9**, 105 (1994).
[19] J. C. Mikkelsen, Jr., MRS Proc. **59**, 19 (1985).
[20] J. Vanhellemont, J. Appl. Phys. **78**, 4297 (1995).
[21] A. Haarahiltunen, H. Väinölä, M. Yli-Koski, R. Ruotsalainen, E. Saarnilehto, S. Kaarlela, E. Haimi, and J. Sinkkonen, in: Microscopy of Semiconducting Materials 2003, edited by A. G. Cullis and P. A. Midgley (Institute of Physics Publishing, Bristol, 2003), p. 417.
[22] N. Streckfuß, L. Frey, G. Zielonka, F. Kroninger, C. Ryzlewicz, and H. Ryssel, Fresenius J. Anal. Chem. **343**, 765 (1992).
[23] M. B. Shabani, Y. Shiina, F. G. Kirscht, and Y. Shimanuki, Mater. Sci. Eng. B **102**, 238 (2003).
[24] M. B. Shabani, T. Yoshimi, and H. Abe, J. Electrochem. Soc. **143**, 2025 (1996).
[25] A. Haarahiltunen, H. Väinölä, O. Anttila, E. Saarnilehto, M. Yli-Koski, J. Storgårds, and J. Sinkkonen, Appl. Phys. Lett. **87**, 151908 (2005).
[26] H. Hieslmair, S. Balasubramanian, A. A. Istratov, and E. R. Weber, Semicond. Sci. Technol. **16**, 567 (2001).
[27] A. A. Istratov, W. Huber, and E. R. Weber, J. Electrochem. Soc. **150**, G244 (2003).
[28] H. Kohno, H. Hieslmair, A. A. Istratov, and E. R. Weber, Appl. Phys. Lett. **76**, 2734 (2000).
[29] K. Honda, A. Ohsawa, and N. Toyokura, Appl. Phys. Lett. **46**, 582 (1985).
[30] Y. Takamura, S. H. Jain, P. B. Griffin, and J. D. Plummer, J. Appl. Phys. **92**, 230 (2002).
[31] Y. Takamura, P. B. Griffin, and J. D. Plummer, J. Appl. Phys. **92**, 235 (2002).
[32] A. Haarahiltunen, H. Talvitie, H. Savin, O. Anttila, M. Yli-Koski, M. I. Asghar, and J. Sinkkonen, J. Mater. Sci.: Mater. Electron. **19**, S41 (2008).
[33] A. Haarahiltunen, H. Talvitie, H. Savin, M. Yli-Koski, M. I. Asghar, and J. Sinkkonen, Appl. Phys. Lett. **92**, 021902 (2008).
[34] J. L. Benton, P. A. Stolk, D. J. Eaglesham, D. C. Jacobson, J.-Y. Cheng, J. M. Poate, N. T. Ha, T. E. Haynes, and S. M. Myers, J. Appl. Phys. **80**, 3275 (1996).
[35] P. A. Stolk, J. L. Benton, D. J. Eaglesham, D. C. Jacobson, J.-Y. Cheng, J. M. Poate, S. M. Myers, and T. E. Haynes, Appl. Phys. Lett. **68**, 51 (1996).
[36] J. L. Benton, P. A. Stolk, D. J. Eaglesham, D. C. Jacobson, J. Y. Cheng, J. M. Poate, S. M. Myers, and T. E. Haynes, J. Electrochem. Soc. **143**, 1406 (1996).

